MESSIAH UNIVERSITY

Messiah University
Mosaic

Honors Projects and Presentations: Undergraduate

Spring 5-2018

Growth and Characterization of ZnSe Thin Films by RF Magnetron Co-Sputtering

Hallie Miller

Follow this and additional works at: https://mosaic.messiah.edu/honors

 Part of the Physics Commons

Permanent URL: https://mosaic.messiah.edu/honors/43

Recommended Citation

Miller, Hallie, "Growth and Characterization of ZnSe Thin Films by RF Magnetron Co-Sputtering" (2018). *Honors Projects and Presentations: Undergraduate*. 43.
https://mosaic.messiah.edu/honors/43

Sharpening Intellect | Deepening Christian Faith | Inspiring Action

Messiah University is a Christian university of the liberal and applied arts and sciences. Our mission is to educate men and women toward maturity of intellect, character and Christian faith in preparation for lives of service, leadership and reconciliation in church and society.

www.Messiah.edu One University Ave. | Mechanicsburg PA 17055

Growth and Characterization of ZnSe Thin Films by RF Magnetron Co-Sputtering

Hallie Miller

Dr. Hellgren

Honors Project in the Department of Mathematics, Physics and Statistics,

Messiah College, May 2018

Zinc-selenide, ZnSe, is a II-IV semiconductor that is known for its wide bandgap of ~2.6 eV. In the growing world of advanced electronics, ZnSe thin films are useful to study in order to widen our understanding of semiconductor physics and to enable us to create and develop higher preforming electronics. In this study, we have grown ZnSe thin films by radio frequency (RF) magnetron sputtering. We are specifically seeking to understand how the ratio of Zinc to Selenium, and the temperature the films are grown at, affects the bandgap and crystalline structure. Ten different ratios of Zn to Se were grown, to a thickness of roughly 300 nm, with each ratio being grown in room temperature and 300 °C, respectively. The band gap was determined using Ultraviolet Visible spectroscopy (UV-Vis) and the crystalline structure was determined using X-Ray diffraction (XRD). The bandgap was not affected by the change in temperature, but it was affected by the ratio of Zinc to Selenium.

1. Introduction

Wide band gap (WBG) semiconductors are gaining interest in the scientific community as a potential replacement for silicon semiconductors. Some of the most commonly investigated WBG semiconductors are SiC, GaN, and ZnO [1]. WBG semiconductors have the potential to have a higher energy efficiency yield than their silicon counterparts. WBG semiconductors have band gaps ranging from ~2.3 – 4.0 eV, in comparison to silicon which has a bandgap of 1.1 eV [2]. This larger band gap enables these devices to withstand higher voltages, which allows for the production of much thinner semiconductors than previously accomplished with silicon. Thinness is desirable because it allows for faster switching and lower resistance [2]. Devices with lower resistance produce less heat while the device is in use which results in a lower energy consumption [2]. These factors make WBG semiconductors more energy efficient than silicon semiconductors because less power is used in switching. The thermoelectric properties of WBG semiconductors are also being investigated [1]. WBG semiconductors are currently being researched for their uses in electric vehicles [2] and high temperature thermoelectrics [1].

ZnSe is a II-VI semiconductor that is interesting to study because of its transparency in the infrared zone and its operation in the blue zone [4]. This makes it an exciting material to study for its potential to be used for high-performance optoelectronics devices, which includes laser diodes and light emitting diodes [4]. ZnSe is also of interest because it is used as a substrate for self-assembling monolayers. However, the bulk form of ZnSe often has too rough of a surface, which makes it harder to use. By growing ZnSe in thin films the surface roughness can be decreased, making them useable as a substrate.

Typical growth methods for WBG semiconductors come in two categories, bulk growth methods and film growth methods. Although films are used for the application side of WBG semiconductors, the bulk growth methods of ZnSe are equally important because high purity bulk crystals are necessary for improving electronic devices, since film growth is often dependent on using high purity bulk crystals [4]. The most common bulk crystal growth method is chemical vapor transport (CVT). This has the advantage that it can be grown at low temperatures which can prevent phase transition and contamination [4]. The second most common bulk growth method is physical vapor transport (PVT). PVT is useful for II-VI semiconductors because it uses the volatility of the two elements to its advantage whereas in other growth methods this volatility makes growing the bulk crystal difficult. This method is usually done below the melting point of the materials which reduces defects [4]. Films are commonly grown using epitaxy techniques, which means that crystalline films are deposited onto substrate of the same, or very similar, crystalline structure [4]. Epitaxy growth methods grow films from the liquid and vapor phase. Liquid Phase Epitaxy (LPE) is grown from the liquid phase and has the advantage of high purity and being grown at low temperature. However, it is hard to increase the thickness of the material, and the surface morphology is poor [4]. Growth from the vapor phase commonly takes the form of physical vapor deposition (PVD) or chemical vapor deposition (CVD). In both methods films are grown by the deposition of atoms from the vapor phase, the difference being that in CVD, the precursor material is in the form of molecules which chemically react to form a film, while in PVD, the material has to physically be ejected from a solid source. [4]. Growth from the vapor phase is

the most common growth method for II-VI semiconductors because it is an easier technique, with easier composition control, and higher growth rate [4].

The films we grew where grown using Radio Frequency (RF) Magnetron co-sputtering from a combination of Zn, Se and ZnSe targets. This growth method was an area of interest to us as ZnSe has not been widely grown using this method before. We explored how the temperature of the substrate, and ratio of Zn to Se, affects the bandgap and crystalline structure of the films. Our purpose was to determine how the bandgap was affected by these conditions so that we can fine-tune the bandgap of ZnSe films.

2. Experimental Details

The ZnSe films were grown using RF Magnetron sputtering and were characterized using Ultraviolet Visible Spectroscopy (UV-VIS), X-Ray Diffraction (XRD), X-Ray Photoelectron Spectroscopy (XPS) and Ellipsometry. In this section, I will briefly describe the techniques in general, and give specific details for the experiments used in this study.

2.1 Film Growth

2.1.1 RF Magnetron Sputtering

Magnetron Sputtering is a thin film deposition technique in which films are grown on a substrate atom by atom. A schematic of a magnetron sputtering system is shown in Figure 1. Disks of the material that will be deposited are mounted on the magnetrons, which can be seen in the bottom of the figure. Each of these magnetrons has a negative potential (typically several hundred volts) applied to them, making each target a cathode. This creates an electric field within the chamber, which is used to ionize the argon gas in the chamber which creates ions and electrons. Permanent magnets, positioned behind the target in the magnetron, create a magnetic field which trap the electrons in front of the target. By trapping the electrons in the magnetic fields, they continue to collide with the argon gas which results in the creation of more ions, and a sustained glow-discharge plasma is formed, which can be seen near the magnetrons in the Figure 1. The ions are accelerated toward the magnetrons by the electric field, where they collide with the targets and, due to the high energy impact, atoms from the target material are ejected. These atoms are then free to move around the chamber and some eventually deposit on the substrate, which is located at the top of the vacuum chamber.

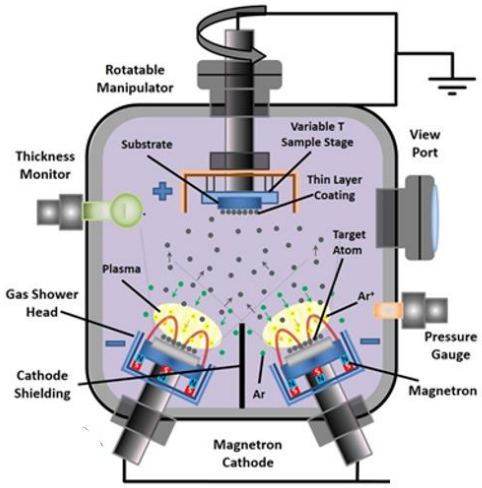

Figure 1: *Schematic of a magnetron sputtering system.*

RF magnetron sputtering works in the same way, but instead of applying a constant voltage to the magnetron, an alternating voltage, in the radio frequency (RF) range (typically 13.56 MHz), is used. RF sputtering must be used for insulating targets, such as ZnSe, to avoid charge build-up. Sputtering occurs when the voltage is negative, but then a negative potential is built up on the target, which repels further Ar^+ ions. However, when the voltage turns positive electrons are attracted which neutralizes the target. In order to optimize the power that actually goes to the plasma, rather than being lost in the wiring between the power supply and magnetron, a tuning system consisting of two variable capacitors (load and tune), is incorporated, as illustrated in Figure 2. The tune and load capacitor affect the deposition rate of each target.

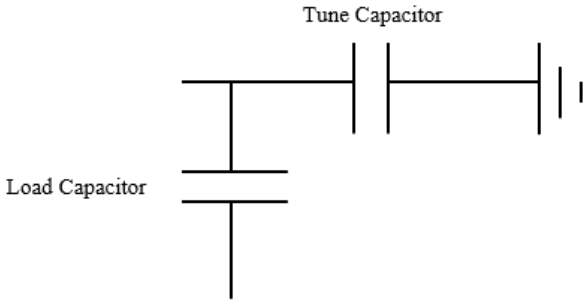

Figure 2: *Schematic of tune and load capacitor for the RF Magnetron Deposition system.*

In this work, we used a BOC Edwards Auto 500 Magnetron Deposition system, with a base pressure of ~10^{-7} Torr (1.3×10^{-5} Pa). All depositions were made a constant pressure of 3 mTorr (0.4 Pa) of argon (99.995% purity, Roberts Oxygen, Rockville, MD). The targets were 99.99% pure ZnSe, Zn and Se disks (Stanford Advanced Materials, Lake Forest, CA), 6 mm thick and 76 mm in diameter. Since two targets were used at the same time (ZnSe and either Zn or Se), a chimney was placed on the ZnSe target to reduce cross-contamination between the targets. A

Dressler Cesar RF power generator was used as the power source for each of the magnetron targets.

2.1.2 Deposition Rate Calibration

Before growing the films, it was first necessary to determine under which conditions a plasma can be formed, and the deposition rate of each target material, Zn, Se, and ZnSe, under those conditions. The deposition rate was determined using a quartz crystal microbalance (QCM), positioned in the center of the substrate holder. The QCM measures the deposition rate by measuring the change in vibrational frequency of the crystal lattice. As more mass is deposited on the Quartz Crystal, the vibrational frequency changes in proportion to the amount of mass added. The change of frequency is then converted to the deposition rate using an Edwards FTM7.

Table 1 shows the parameters that define the power range which gives a sustainable plasma, as well as deposition rate for each of the three targets, Zn, Se, and ZnSe. If the power is too low, the degree of ionization is not sufficient to sustain a plasma, whereas if it is too high, the target starts sparking due to too high ionization. This is especially true for the Se target, due to its low melting point of 220 °C. All deposition rates were determined using a pressure of 3 mTorr of argon gas. Furthermore, it was determined the tune and load capacitance also affect the deposition rate, so they were held constant for power to be the only independent variable. The tune and load capacitance are different for each target, however for each target they are held constant as the power is changed. After finding this range, we measured the deposition rates at intervals of power, and the results are presented in Figure 3, and summarized in table 1.

Target	Power Range (Watt)	Load Capacitance	Tune Capacitance	Deposition Rate nm/(minW)
Zinc	50-200	61.8%	13.8%	0.1295
Selenium	25-60	85.2%	15.3%	0.0639
ZnSe	50-125	72.2%	13.2%	0.0985

Table 1: *Power ranges that give sustainable plasma, load and tune capacitances, and deposition rates as a function of power for the three targets Zn, Se and ZnSe.*

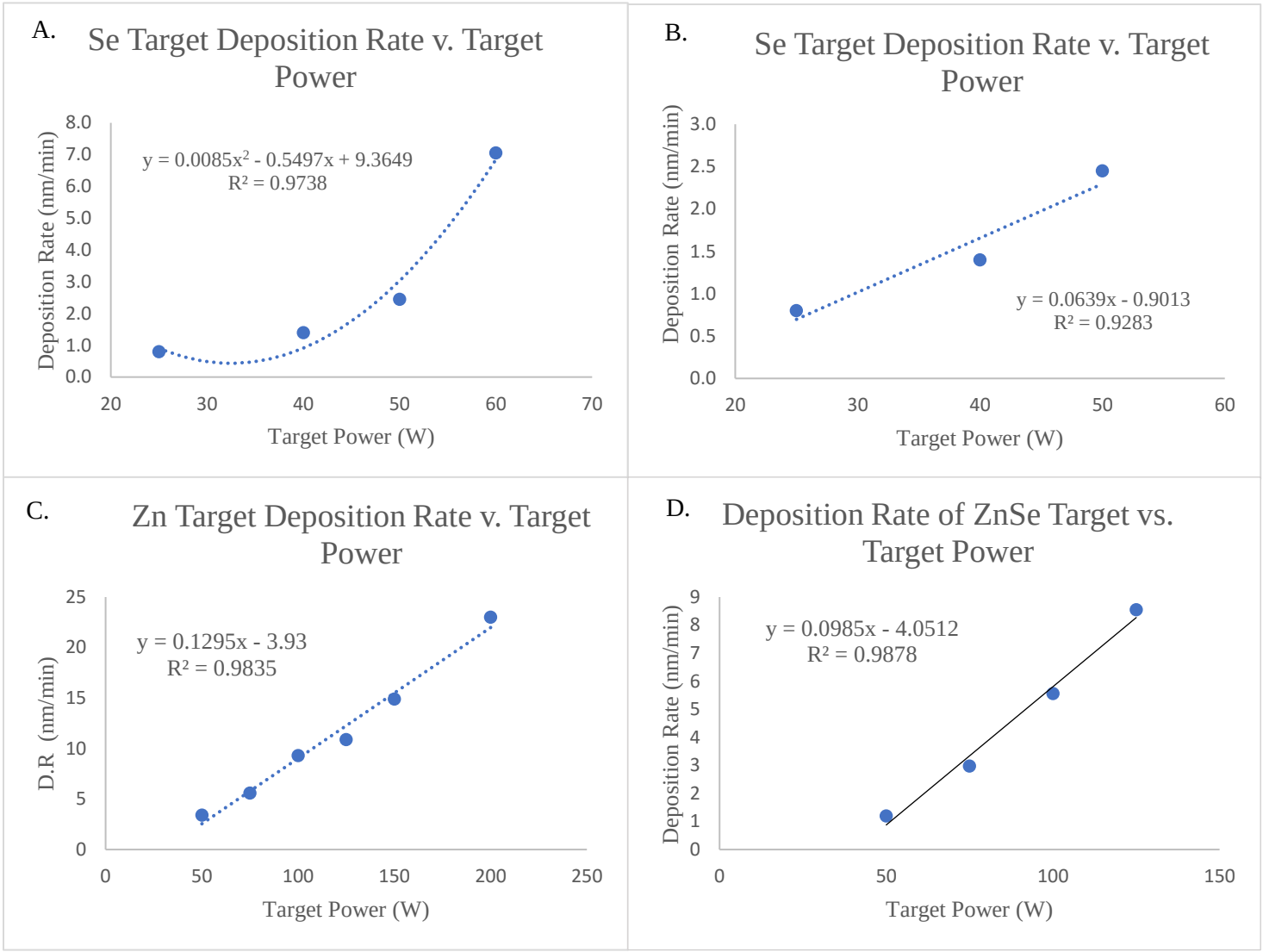

Figure 3: *Deposition rate vs power for A) the Se target with nonlinear fit, B) the Se target subset, with linear fit, C) the Zn target with linear fit, and D) the ZnSe target, with linear fit.*

2.1.3 Film Growth

The ZnSe films were grown on glass and silicon substrates. Glass was chosen because a transparent substrate is necessary to determine the bandgap using UV-VIS. Silicon was chosen as substrate for all other analysis. Five films were grown at a time, resulting in five sample from each ratio, three films were grown on glass substrate, and two were grown on silicon substrates. The orientation of the substrate is shown in Figure 4. The substrate holder did not rotate, therefore some of the films were grown more directly over the respective targets, which resulted in slightly different Zn/Se ratio. In the center of the substrate holder, there were two silicon substrates and one glass substrate. The glass substrate was positioned in the center of the holder,

with silicon substrates located at each side. The two additional glass substrates where positioned at opposite edges of the holder to see if the bandgap was affected by small variations in the ratio of Zn to Se.

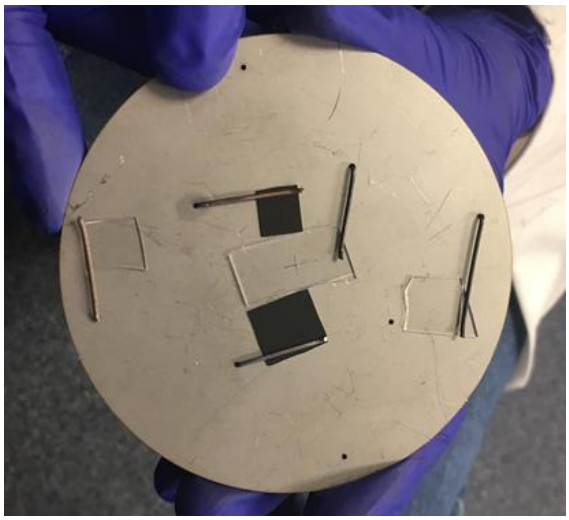

Figure 4: *Layout of the substrate mounting used to grow ZnSe. The disk is 3 inches in diameter.*

In table 2 the ten ratios of Zn to Se are listed along with the two targets used to grow them. This table gives the estimated time needed to grow the film to the thickness of 300 nm. Each ratio was grown at ambient temperature and 300 °C.

Target Ratio Zn:Se	Se Power	ZnSe Power	Zn Power	Growth time min
1:6	53 W	51 W		86
1:3	53 W	67 W		40
1:2	53 W	92 W		40
1:1		92 W		60
2:1	53 W		69 W	40
3:1	53 W		88 W	30
6:1	53 W		146 W	17
9:1	34 W		117 W	24
12:1	34 W		146 W	18.5

Table 2*: The targeted ratios of ZnSe and the power and time needed to grow them.*

2.2 Film Characterization

2.2.1 X-ray Photoelectron Spectroscopy (XPS)

X-ray photoelectron spectroscopy is a characterization technique shown in Figure 5 that uses the photoelectric effect to find the surface characteristics of a film. The photoelectric effect describes how electrons can be freed from a material when light is shone on it at certain frequencies. This phenomenon is called photoemission and is described by equation 1 [9]:

$$E_{h\nu} = E_{\varphi} + E_k + E_b \qquad \textbf{Equation 1}$$

Here $E_{h\nu}$ is the energy of the incident x-rays, $E_{\varphi}$is the work function, E_k is the kinetic energy of the freed electron, and $E_b$is the electron binding energy [9]. A visual of this equation can be seen in Figure 6. The film is irradiated with x-rays and the kinetic energy of the photelectrons electrons is recorded. The energy of the x-ray, work function, and kinetic energy are then used to calculate the binding energy using equation 1.

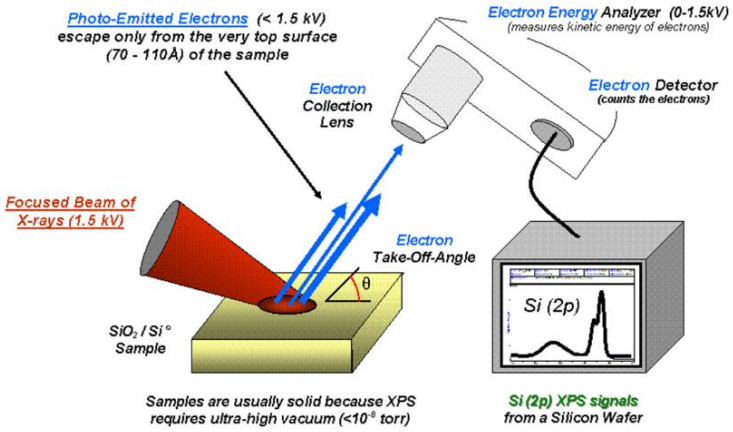

Figure 5: *Schematic of XPS operations [12]*

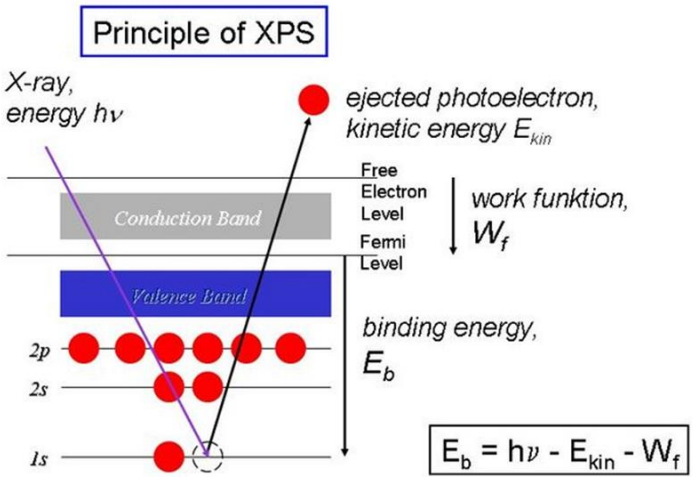

Figure 6: *Schematic of energy levels in XPS. The energy levels correspond to the energy of the x-ray, binding energy, kinetic energy of the freed electron, and the work function. [12]*

X-ray photoelectron spectra for two of our films, with different Zn/Se ratio, is shown in Figure 7. Each element has specific binding energies, so by comparing the peak positions to known databases, the elements of the film can be determined. Furthermore, the intensity of each peak is

proportional to the concentration of that element, as can be seen in Figure 7, where Zn_6Se (blue spectra) has significantly higher peaks corresponding to Zn, and the $ZnSe_6$ has larger Se peaks. Peaks corresponding to carbon and oxygen can also be seen. They are due to surface contaminations due to the samples being exposed to the atmosphere after deposition.

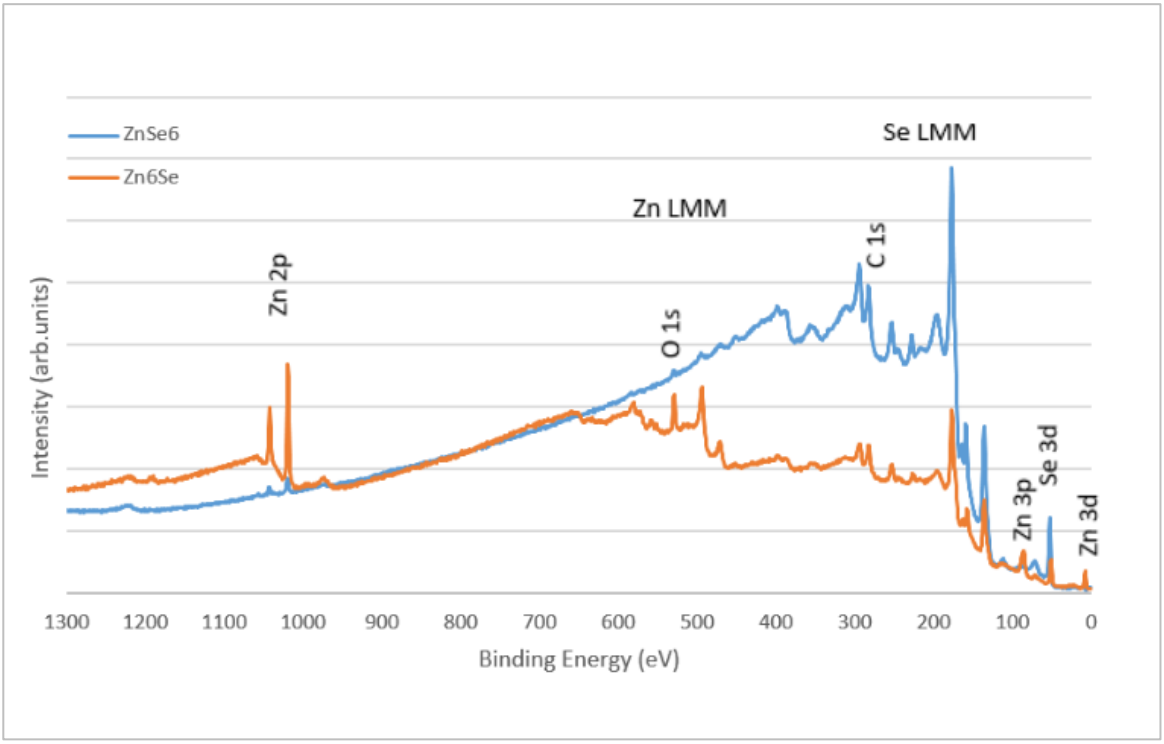

Figure 7: *X-ray photoelectron spectra of two films; ZnSe6 and Zn_6Se. The Se 3d peak is higher for $ZnSe_6$, and the Zn 2p, 3p, and 3d are higher for Zn_6Se as expected.*

Our measurements were done on a Phi VersaProbe II instrument at the Materials Research Institute at the Penn State University. The instrument was equipped with a monochromated Al K_α x-ray source, $E_{h\upsilon} = 1486.7\ eV$. Data was processed using the CasaXPS software package.

2.2.2 X-Ray Diffraction

X-ray Diffraction (XRD) is used to find the crystalline structure of a sample. XRD works by irradiating samples with electromagnetic waves in the X-ray spectrum and recording the intensity of X-rays that are scattered at each angle. Figure 8 shows a schematic of XRD. The X-rays are incident at angle θ, while the sample is rotated at the same angle. Thus, the angle between the incoming and diffracted beam is 2θ. The x-rays only scatter when they encounter an atom, and x-rays scattering off the atoms only form constructive interference at certain angles, when Bragg's law is satisfied:

$$2d \sin\theta = n\lambda \qquad \textbf{Equation 2}$$

where λ is the wavelength of the incident x-ray, d is the distance between the atomic planes in the crystal, and n is an integer representing the order of diffraction. We can either calculate the inter-atomic distance using Bragg's law, or compare the scattering angles to known XRD reference data to identify the peaks in our data. If no scattering peaks are found it means the structure is amorphous and the atoms are arranged randomly throughout the sample.

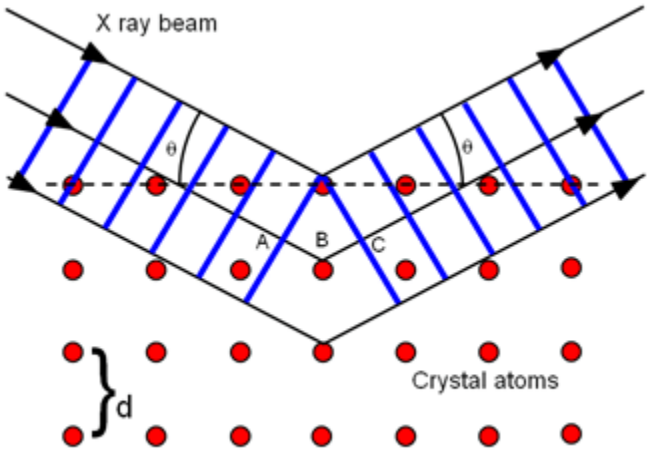

Figure 8: *Schematic of XRD. X-Ray beams are scattered off crystal atoms and the reflection angle tell us the structure of the sample [13].*

Measurements were done using the Rigaku Miniflex II, operating with Cu K_α x-ray source ($\lambda = 1.54$ Å), located in the Chemistry Department of Messiah College.

2.2.3 Ultraviolet Visible Spectroscopy

Ultraviolet Visible (UV-VIS) Spectroscopy measures the absorbance spectrum of a sample. UV-VIS radiates the sample with light in the 100-1000 nm range and records the absorption intensity at each wavelength. As shown in Figure 9, light is incident on a dispersion device which splits the light into the visible and ultraviolet light spectrum. In order to find the absorption of the film alone, we first need to measure the absorption of a bare substrate, as a baseline. Any additional absorbance recorded for the coated substrate will correspond to the film.

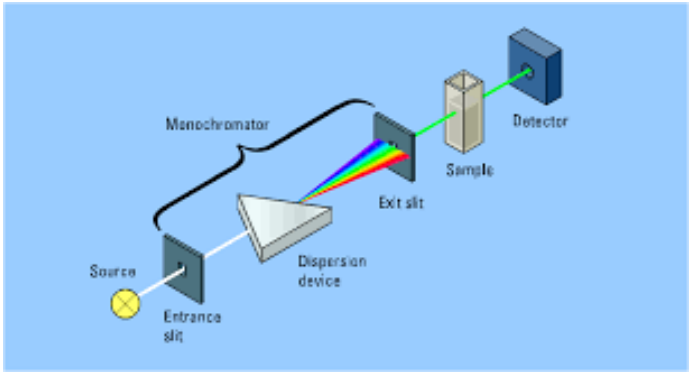

Figure 9: *Schematic of UV-VIS [14].*

The absorbance spectrum of a sample can be used to determine the bandgap of the sample, by converting it to a so-called Tauc plot [6]. A Tauc plot is made by taking the square root of the absorption multiplied by the energy of the light that is being absorbed. This is plotted versus the photon energy. By extrapolating the linear portion of this fit, the energy band-gap is found to be the intercept of the x-axis [6].
In this work we used a Thermo Scientific Evolution 300 Ultraviolet Visible Spectroscopy instrument to perform the absorption spectrum. We specifically looked at the region of absorption from 300-900 nm.

2.2.4 Spectroscopic Ellipsometry

Spectroscopic Ellipsometry is used to find the thickness and optical constants, such as refractive index and bandgap of the films. This technique is shown in Figure 10. It works by measuring the changes in polarization of light that is reflected or transmitted by the film [10]. A beam of light is first polarized and then allowed to shine on the sample. The resulting reflection then goes through another polarizer which measure the change in polarization from being reflected by the sample. This change can then be used, by fitting a model, to determine the thickness, refractive index, and bandgap of the film [10].

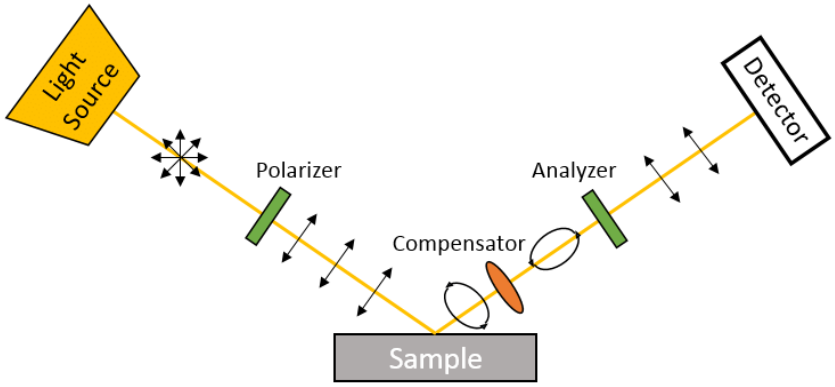

Figure 10: *Schematic of spectropic ellipsometry [15].*

In this work, a Mueller matrix dual rotating compensator ellipsometer (RC2) from J.A. Woollam Co. was used. Optical constants were measured in the wavelength range 210-1690 nm (0.7-5.9 eV), at angles between 45° and 75°.

3. Results

The films were grown as described in section 2, and then analyzed using XPS, Ellipsometry, XRD and UV-VIS. Figure 11 shows the films grown on glass substrates. The films are organized by targeted ratio of Zn to Se and growth temperature (RT = room temperature, and HT = high temperature, i.e., 300 °C). The films grown at high temperature in most cases are significantly thinner than their ambient temperature counter parts. The RT-

grown films with higher levels of Se (Zn/Se ≤ 1:2), appear opaque, but if held up to the light, they do transmit in the red range, but the absorbance is high. From Zn/Se 1:1 to 6:1, the films are different shades of yellow, which is more similar to the yellow of bulk ZnSe. At ratios of Zn/Se ≥ 9, the films become metallic and do not transmit light.

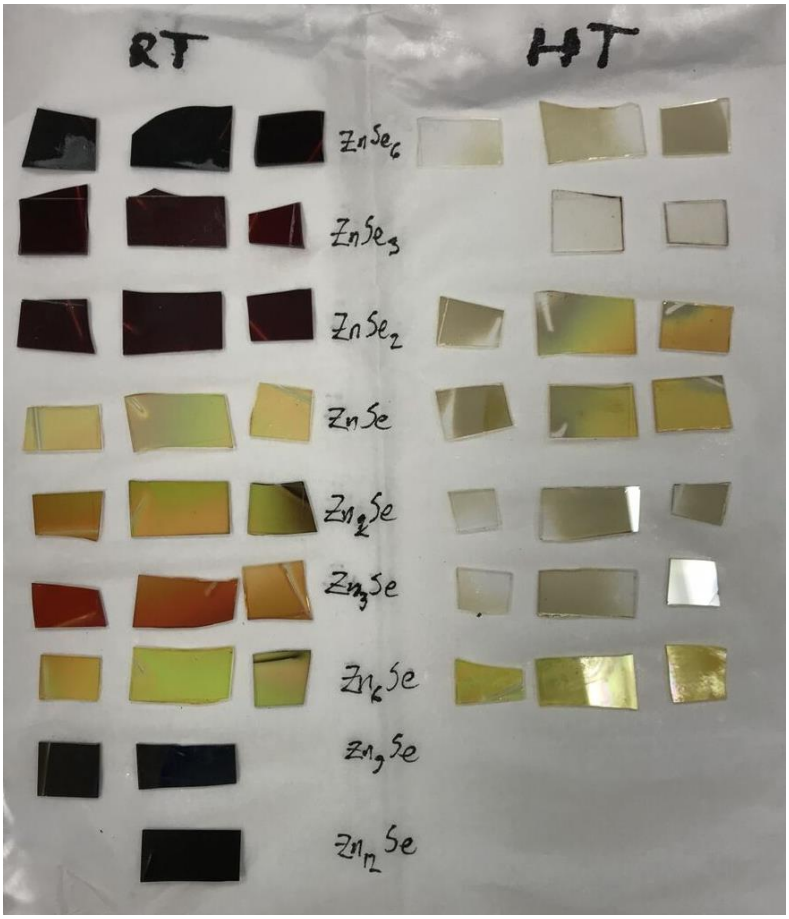

Figure 11: *The films grown on glass substrates organized by intended Zn/Se ratio, grown at room temperature (RT) and high temperature (HT), i.e., 300°C.*

3.1 Composition

Figure 12 shows the actual ratio of Zn/Se achieved vs. the targeted ratio, as measured by XPS, for films grown at ambient temperature and high temperature. The achieved ratio of Zn/Se is significantly different than the targeted. The goal was to grow 10 different ratios of Zn/Se, instead there are three regions where the ratio plateau's. The first plateau region occurs in the ratio of Zn/Se 1:6-1:2 in which the actual ratio was roughly 1:4. The second plateau region occurs at Zn/Se ratio 1:1-6:1, where the achieved ratio is roughly 1.5:1. The last region occurs at Zn/Se ratio 9:1 and above, where the achieved ratio is approaching 20:1 (not graphed in Figure 12). This occurs because below and above the 1:1 ratio of Zn/Se, the film has a preferred structure. The ratio that occurs is the most energetically favorable regardless of how much Zn or Se is bombarding the substrate. The excess Se or Zn does not deposit on the substrate but goes

back into the gas phase and is pumped away. It is also noted that a 1:1 ratio of ZnSe is never achieved, even when the ZnSe target is the only target being used to grow a film.

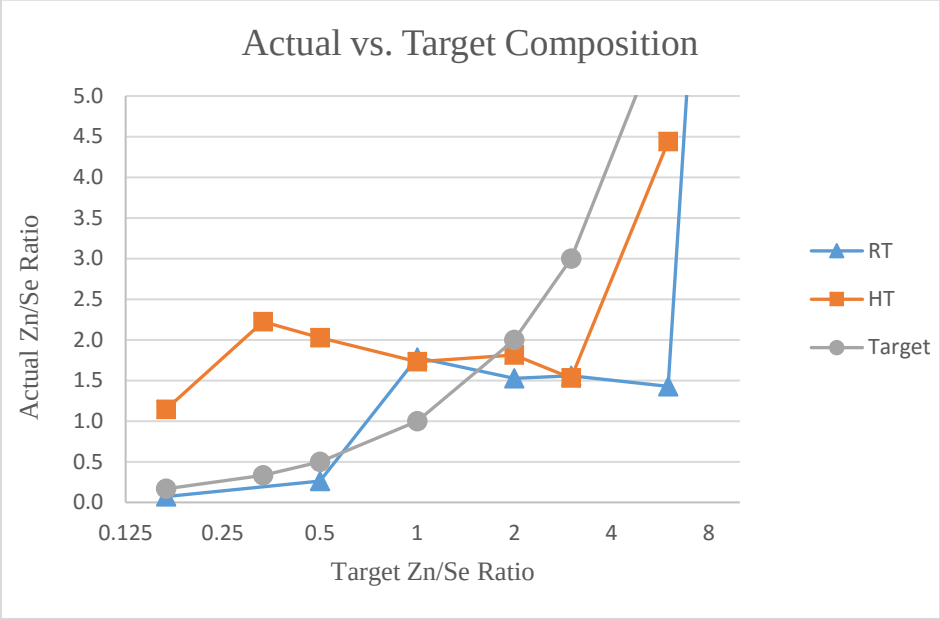

Figure 12: *The actual ratio of Zn/Se vs. the target ratio*

Figure 13 compares the thickness of the films grown at ambient temperature versus high temperature. As mentioned above, the films grown at high temperature were significantly thinner than their room temperature counterparts, which can be seen in Figure 11 and 13. The thinness of high temperature films makes them harder to analyze and makes their data more uncertain. Therefore, even though films were grown at both high and low temperature, we will henceforth focus on the films grown at room temperature.

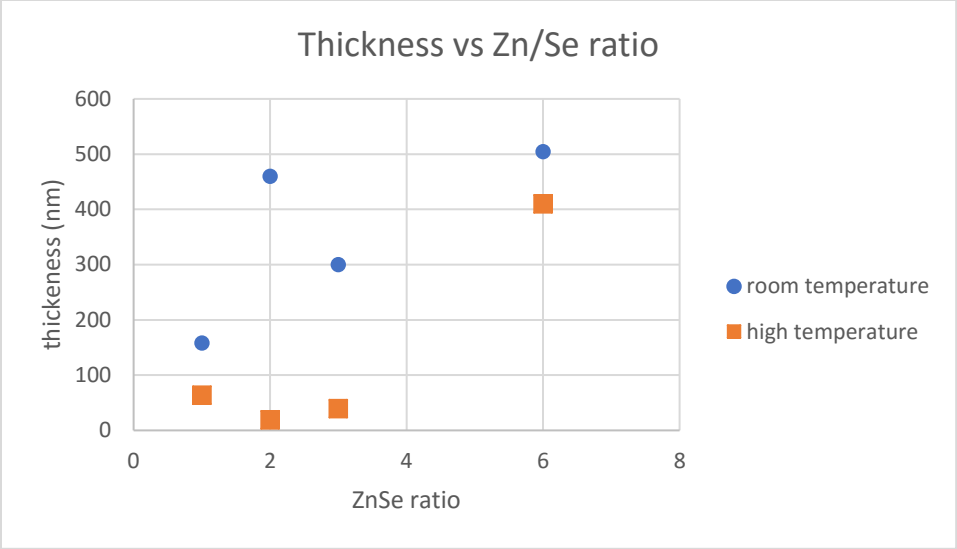

Figure 13: *Film thickness vs the target Zn/Se ratio for films grown at room temperature and high temperature*

3.2 Structure

Figure 14 shows the diffraction peaks obtained using XRD. This graph includes all ratios of Zn/Se that were grown at room temperature. At concentrations of Zn to Se 9 and higher, the diffraction peaks emerging at 2θ angles of 36°, 38°, and 45°, which correspond to the crystalline

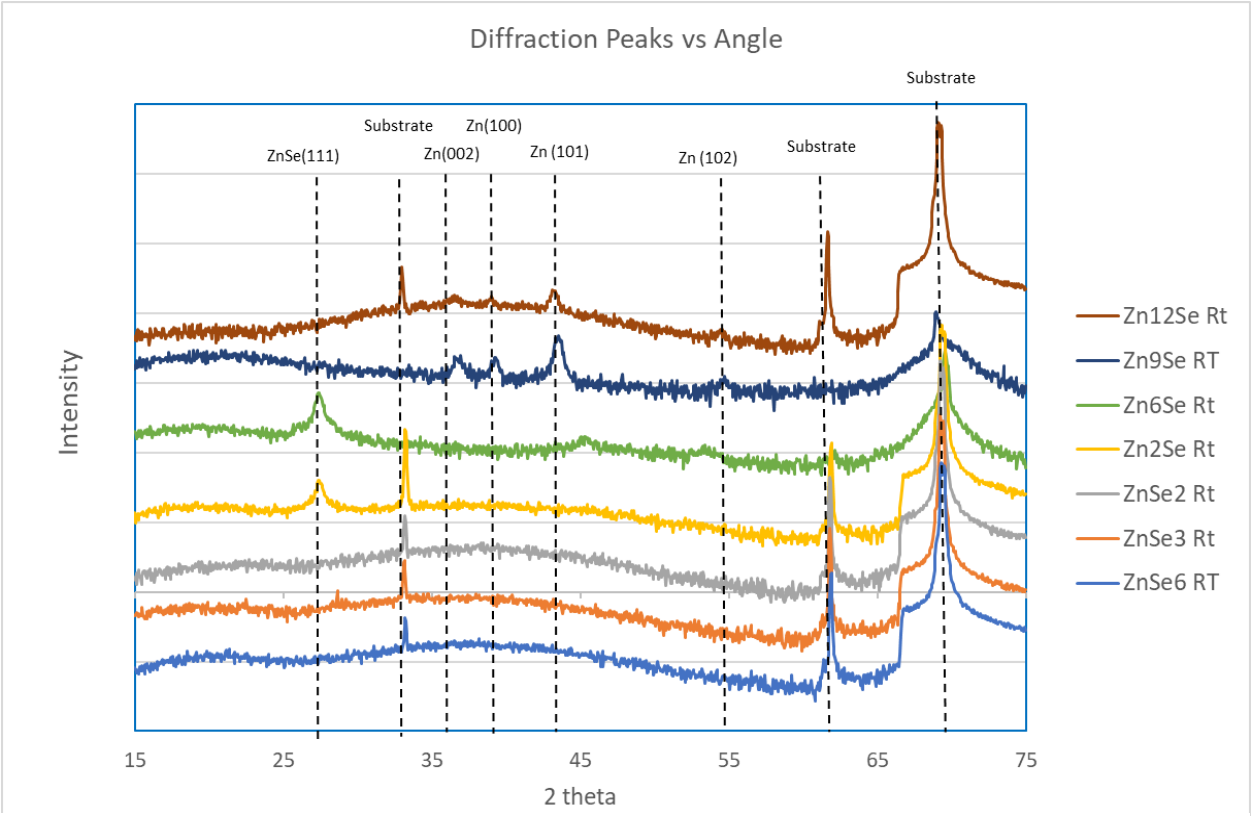

Figure 14: *X-ray diffractograms comparing all films grown at room temperature*

structure of Zn. At ratios of Zn to Se 6 to 2, the diffraction peaks correspond to the structure of ZnSe, specifically the peak present at 28 degrees. At ratios of Se to Zn or 2 and higher, no diffraction peaks are present except for the ones corresponding to the substrate. This means at higher levels of Se, the structure is amorphous, and the atoms have a random orientation. When compared to the XPS data found in 3.1, the structure of the films corresponds to the three regions of achieved ratio.

3.3 Refractive Index

Figure 15 shows the relationship between the refractive index (n) and the Zn/Se ratio found using Ellipsometry. Films with a higher concentration of Se have a higher refractive index, and films with a higher concentration of Zn have a lower refractive index. There is not a clear distinction between the three regions of achieved ratio of Zn/Se.

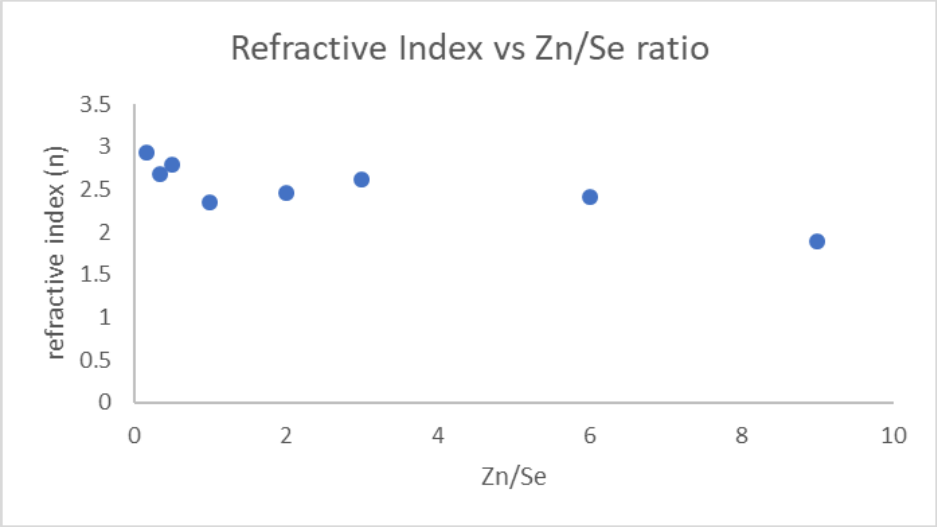

Figure 15: *The refractive index vs the ratio of Zn/Se.*

3.4 Bandgap

Two methods were used to determine the bandgap, ellipsometry and UV-VIS. Figure 16 compares the bandgap determined using ellipsometry and UV-VIS vs the achieved ratio of Zn/Se found in section 4.1 using XPS. Looking at the size of the bandgap found using Ellipsometry, it again comes in three distinct areas of bandgap that correspond with the three regions of achieved ratio. The bandgap at higher ratios of Se is approximately 2.0 eV. As the amount of Zn increased, the bandgap increases to 2.2-2.5 eV, with a slight increase in bandgap size with increase in Zn. At high levels of Zn, the bandgap drops to zero, which corresponds to the metallic nature of Zinc.

The bandgap found using UV-VIS has similar trends, with slightly lower overall bandgaps. The bandgap at high levels of zinc are not shown but are zero. There are three regions of bandgap,

like what is found using Ellipsometry. The first region occurs at high levels of Se and is approximately 1.8-1.9 eV. The next region is at an approximate Zn/Se ratio of 1.5:1, and ranges from 1.6-2.1 eV. This follows the trend of having smaller bandgaps at higher ratios of Se/Zn, larger bandgaps at ratios of Zinc 1.5:1, and no bandgap at ratios of Zn/Se 9 and higher.

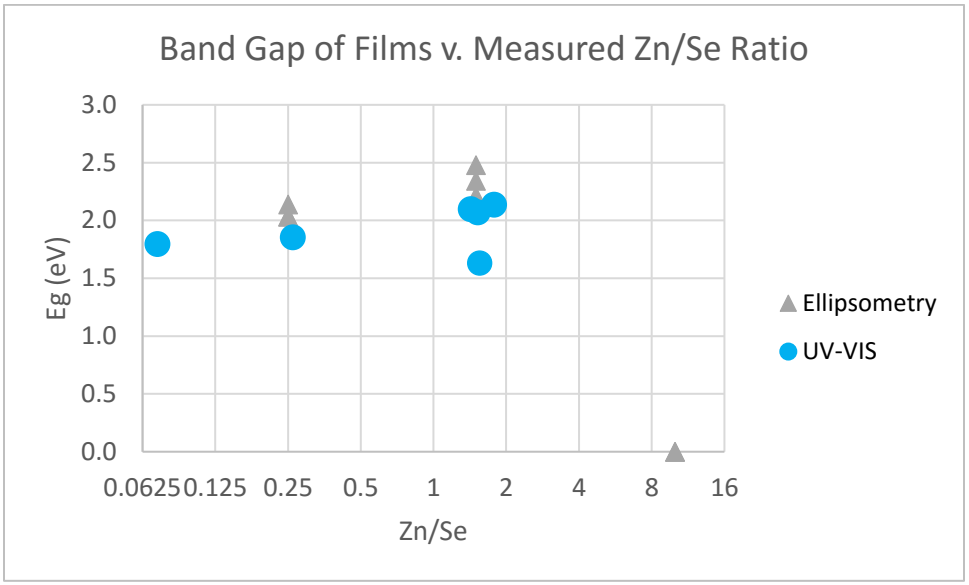

Figure 16 *Compares the Bandgap vs achieved ratio of Zn/Se found using Ellipsometry and UV-VIS.*

4. Summary and Conclusions

ZnSe thin films where grown with ten different ratios of Zn to Se. The purpose was to determine if the composition, structure, refractive index and bandgap change based on the ratio. The bandgap, crystalline structure, and refractive index where found using XRD, UV-VIS, XPS, and Ellipsometry. XPS was used to determine the achieved ratio of Zn/Se compared to the target. It was found the ratio of Zn/Se cannot be changed by increasing the deposition flux, instead the ratio is found in three distinct regions. The structure was found using XRD, 3 different structures were found which correlate to the three ratios achieved. With a higher ratio of Zn the structure shows diffraction peaks corresponding to Zn structure. At the ratio of Zn_6Se to Zn_2Se the structure corresponds to ZnSe structure. With ratios of $ZnSe_6$ to $ZnSe_2$ the structure has no diffraction peaks indicating the structure is amorphous. The refractive index, as measured by ellipsometry, increases with an increasing ratio of Se and decreases with an increasing ratio of Zn and is shown in Figure 15. The bandgap was found using UV-VIS and Ellipsometry. The bandgap was found to be smaller at higher ratios of Se, larger at ratios of Zn_6Se to Zn_2Se and zero at ratios of Zn_9Se and higher. Overall, the bandgap did not change drastically, but did follow a trend.

5. Acknowledgements

I would like to thank my advisor Dr. Hellgren for his guidance on this project and continued support. I would also like to thank my lab partner, Alex Sredenschek, for his help growing and analyzing the films. Additionally, the Messiah College Chemistry Department for their use of the XRD and UV-VIS. Penn State Center for Nanoscale Science NSF-MRSEC (DRM-8020404) and Jeff Shallenberger, for use of XPS, and the Thin Film Optics Group at Linköping University, Sweden, for the use of the ellipsometry. Finally, we would like to thank the Intel Corporation for the donation of the deposition system.

6. References

1. Huang, Zheng, et al. "Thermoelectric properties of the 3C, 2H, 4H, and 6H polytypes of the wide-band-gap semiconductors SiC, GaN, and ZnO." AIP Advances 5.9 (2015): 097204.
2. Warren, Joshua A., et al. "Energy impacts of wide band gap semiconductors in US light-duty electric vehicle fleet." *Environmental science & technology* 49.17 (2015): 10294-10302.
3. Ou, Kai, et al. "A study of structural, morphological and optical properties of nanostructured ZnSe/ZnS multilayer thin films." *Journal of Alloys and Compounds* 726 (2017): 707-711. https://www.sciencedirect.com/science/article/pii/S0925838817327640
4. "Wide-Bangap II-VI Semiconductors: Growth and Properties." Springer Handbook of Electronic and Photonic Materials, by Safa Kasap and Peter Capper, Springer US, 2007, pp. 1–19.
5. Natl. Bur. Stand.(U.S) Monogr. 25,13,35,(1976)
6. Rabadanov, M.Kh., Loshmanov, A.A., Shaldin, Yu.V., *Kristallografiya*, **42**, 649, (1997)
7. Kittel, Charles "Introduction to Solid State Physics." by, 8th ed., Wiley, 2005, pp. 1–38.
8. Kawamura, H., Fac. of Science, Himeji Inst. of Technology, Japan., *Private Communication*, (2000)
9. Hollander, Jack M., and William L. Jolly. "X-ray photoelectron spectroscopy." *Accounts of chemical research* 3.6 (1970): 193-200.
10. Hilfiker, James N., et al. "Survey of methods to characterize thin absorbing films with spectroscopic ellipsometry." *Thin Solid Films* 516.22 (2008): 7979-7989.
11. Murphy, A. B. "Band-gap determination from diffuse reflectance measurements of semiconductor films, and application to photoelectrochemical water-splitting." Solar Energy Materials and Solar Cells 91.14 (2007): 1326-1337.
12. "X-Ray Photoelectron Spectroscopy." Wikipedia, Wikimedia Foundation, 23 Apr. 2018, en.wikipedia.org/wiki/X-ray_photoelectron_spectroscopy.
13. Institute of Physics. "X-Ray Diffraction." Episode 530: X-Ray Diffraction, tap.iop.org/atoms/xray/530/page_47297.html.
14. Fog. UV-Vis Absorption Spectroscopy, faculty.sdmiramar.edu/fgarces/labmatters/instruments/uv_vis/cary50.htm.
15. Rosenberg, Aaron & Hu, Dawei & Chouaib, Houssam & Tan, Zhengquan & Malkova, Natalia. (2018). Tracking the defects and the band gap of ultra-thin HfO2 using a multi-oscillator Cody Lorentz model. 102. 10.1117/12.2296980.
16. Swanson, Tatge., *Natl. Bur. Stand. (U.S.), Circ. 539*, **I**, 16, (1953)